

# Mechanism of magnetic phase transition in correlated magnetic metal: insight into itinerant ferromagnet $\text{Fe}_{3-\delta}\text{GeTe}_2$

Yuanji Xu,<sup>1</sup> Yue-Chao Wang,<sup>2</sup> Xintao Jin,<sup>1</sup> Haifeng Liu,<sup>2</sup> Yu Liu,<sup>2</sup> Haifeng Song,<sup>2,\*</sup> and Fuyang Tian<sup>1,†</sup>

<sup>1</sup>*Institute for Applied Physics, University of Science and Technology Beijing, Beijing 100083, China*

<sup>2</sup>*Laboratory of Computational Physics, Institute of Applied Physics and Computational Mathematics, Beijing 100088, China*

(Dated: July 9, 2024)

Developing a comprehensive magnetic theory of correlated itinerant magnets is a challenging task due to the difficulty in reconciling both local moments and itinerant electrons. In this work, we investigate the microscopic process of magnetic phase transition in ferromagnet metal  $\text{Fe}_{3-\delta}\text{GeTe}_2$ . A new paradigm is proposed to describe the magnetic phase transition in correlated metallic ferromagnets, where Hund's coupling dominates the spectral weight transfer between different spin channels, rather than spin-splitting as described by the Stoner model. We recognize that our theory should be universal for itinerant magnets. Additionally, we reveal an efficient way to achieve novel quantum states from various competing orders in multi-site crystal structures. Our research shows that Fe1 are proximate to Mott physics, while Fe2 exhibit Hund physics due to their distinct atomic environments. These competing orders work together to produce heavy fermion behavior within ferromagnetic long-range order through well-defined quasiparticle bands, which are promoted by Hund's coupling and further hybridized with relative itinerant bands. The complex interactions of competing orders drive correlated magnetic metal to a new frontier for discovering outstanding quantum states and exotic phenomena in condensed matter physics.

Magnetism plays a crucial role in condensed matter physics, especially in strongly correlated systems. It is closely linked to various emergent phenomena such as heavy fermion behavior [1, 2], unconventional superconductivity [3, 4], Hund metal [5, 6], and quantum phase transition [7, 8]. These fascinating behaviors arise due to the dual nature of correlated electrons, which creates challenges in understanding the role of magnetism. One essential scenario is the delocalization of  $f$ -electrons at low temperatures in heavy fermion systems, achieved through the hybridization of local moments with conductive electrons via RKKY interaction [9]. Another critical instance is the  $d$ -electron Hund metals, which appear even more mysterious as the systems do not have explicit two fluids [10]. The odd coexistence of itinerant and localized behaviors in Hund metals, dominated by Hund's coupling, has scored significant victories in iron-based superconductors [5, 11–14]. However, from a theoretical perspective, the two commonly used models, one starting from the Heisenberg local moment model and the other from the Stoner itinerant electron model [15, 16], have their limitations in treating these systems. The microscopy mechanism of considering both local moments and itinerant electrons in correlated magnetic metal still needs to be explored.

Recently, van der Walls (vdW) itinerant ferromagnet  $\text{Fe}_3\text{GeTe}_2$  (FGT) has garnered significant attention. It is a potential candidate for voltage-controlled spintronic devices due to its exceptional exfoliation properties and robust high Curie temperature [17, 18]. In bulk material, the ferromagnetic (FM) Curie temperature  $T_c$  is around 220 K, and it can even reach room temperature with an ionic gate in its thin flakes [17, 19, 20]. Furthermore, experiments have observed significant electron mass en-

hancement [20–23], which is also supported by previous theoretical calculations [24]. Considering its high ferromagnetic transition temperature and strongly correlated effects, the itinerant ferromagnet FGT presents an ideal platform for investigating the dual nature of magnetism and its interplay with other exotic phenomena [25].

Here, we highlight some mysteries that may be related to the issue of magnetism in FGT. First and foremost is the question of how to describe the Fe- $d$  electrons accurately. Although the itinerant Stoner model is commonly accepted [20, 26], recent experiments suggest that the Heisenberg model may be necessary to describe the ferromagnetism in FGT correctly [27–30]. For instance, the angle-resolved photoemission spectroscopy (APRES) experiments find that the temperature-dependent evolution towards the ferromagnetic transition is strikingly weak [27, 30]. Secondly, as is commonly discussed in iron-based superconductors [5, 31, 32], it is unclear whether the irons in FGT exhibit Hundness or Mottness. Kim et al. suggest that it is a “site-differentiated” Hund metal [33], while another study suggests that it is close to an orbital selective Mott transition (OSMT) [34]. Finally, previous studies have reported heavy fermion behavior in FGT with a large Sommerfeld coefficient ( $\gamma_0 = 135 \text{ mJ/mol K}^2$ ) [20–22]. This is striking since  $d$ -electron heavy fermion systems are rare [35–37]. While in FGT, heavy fermion behavior appears to be promoted within ferromagnetic order [22]. These controversies encourage us to explore the complex interaction of magnetism with possible Hund, Mott, or Kondo physics in this system.

In this work, we systematically investigate the correlation effects in itinerant ferromagnet  $\text{Fe}_{3-\delta}\text{GeTe}_2$  using density functional theory combined with dynamical mean-field theory (DFT+DMFT). Our findings reveal a

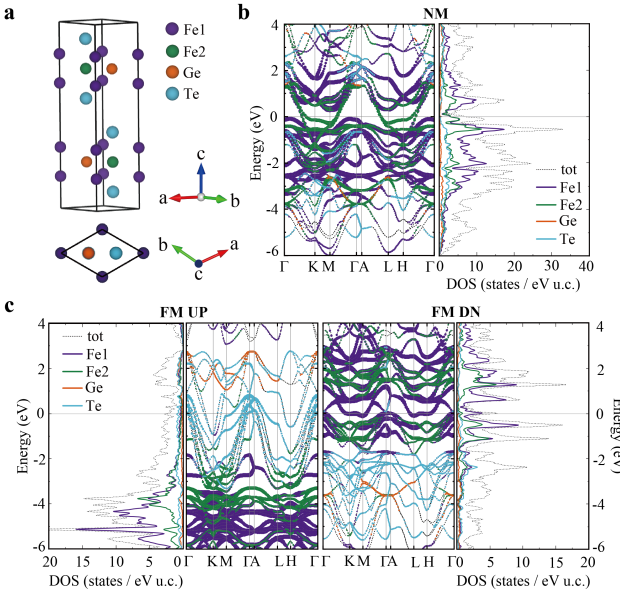


FIG. 1. **Crystal structure and DFT+U electronic structures in FGT.** a, Illustration of the crystal structure of  $\text{Fe}_3\text{GeTe}_2$ . b, The electronic structures and partial density of states of non-spin polarized calculations of  $\text{Fe}_3\text{GeTe}_2$  in DFT+U calculations. c, The electronic structures and partial density of states of ferromagnetic order in DFT+U calculations.

new paradigm of magnetic transition in correlated metallic ferromagnets, characterized by the spectral weight transfer between two spin channels caused by the correlation effect, rather than spin splitting in the mean-field Stoner model. Similarly to Hund metals, the quasiparticles form in itinerant ferromagnet as temperature decreases. Interestingly, the Fe atoms in FGT exhibit two distinct behaviors: one follows Mott physics, while the other exhibits Hundness. This suggests that FGT may be the first material to exhibit both Hundness and Mottness, stemming from the multi-site nature of correlated atoms in its crystal structure. Furthermore, our results demonstrate that Hund's coupling localizes quasiparticles and promotes their hybridization with other itinerant bands, leading to heavy fermion behavior. Our findings not only naturally reconcile the conflicts between heavy fermion behavior and long-range magnetic order, but also open up a new frontier for discovering new quantum states in itinerant magnets.

## Results

### DFT+U calculations

$\text{Fe}_{3-\delta}\text{GeTe}_2$  is a ternary multi-site ferromagnet, as illustrated in Fig. 1a, with layered  $\text{Fe}_3\text{Ge}$  substructures sandwiched by two layers of Te atoms and a vdW gap between adjacent Te layers. FGT crystallizes into a hexagonal structure with the space group of  $P6_3/mmc$  (No.

194), and Fe atoms occupy two inequivalent Wyckoff sites, labeled Fe1 and Fe2. Notably, the occupational deficiency ( $0 < \delta < 0.3$ ) occurs only at the Fe2 site [19, 21]. Our DFT results are consistent with available calculations (Supplementary Information Fig.1) [21, 34]. Considering the strong correlation effects in FGT, we perform DFT+U calculations using the correlation values suggested by previous work [24]. In non-magnetic (NM) calculations, the Fe- $d$  electrons dominate near the Fermi level in Fig. 1b. However, in ferromagnetic order, the correlation effects strongly localize Fe- $d$  electrons, causing the Fe-bands to be pushed away from the Fermi level. As a result, the Fe-bands in the spin-up channel are almost entirely filled and pushed down to 5 eV below the Fermi level, leaving only itinerant bands with Te character in Fig 1c. In contrast, the bands in the spin-down channel move up slightly, leaving a small peak of Fe- $d$  density of states (DOS) at the Fermi level. Besides, the partial DOS of Fe1 and Fe2 have similar peak structures, indicating strong hybridization between them. We note that the DOS at the Fermi level in non-magnetic GGA+U calculations is reduced to 2.9 states/eV f.u., much smaller than 13.6 in GGA calculations [21]. The much smaller DOS in DFT+U calculations, combined with the weak temperature-dependent evolution of Fe- $d$  bands in APRES measurements, suggests to reconsider the application of Stoner model to FGT [27, 30].

### Mechanism of magnetic phase transition using DFT+DMFT calculations

To further explore the electronic structures and magnetism with dynamical correlation effects, we systematically perform DFT+DMFT calculations on FGT [38, 39]. This method has been successfully applied to correlated materials such as Hund metals and heavy fermion materials [5, 9]. For the magnetic calculations using DFT+DMFT, we consider ten Fe- $d$  orbitals and introduce symmetry breaking of the self-energy at the initial stage. As expected, our DFT+DMFT simulations show that the system converges to non-magnetic order at high temperature in Fig. 2a. The spectral function exhibits large blurred regions, and the DOS shows very broad peaks, mainly from the incoherent states of Fe atoms around the Fermi level (from -4 eV to 4 eV). This incoherence arises from the Hubbard bands of Fe atoms, originating from the strong Coulomb interaction. Moreover, the system converges to the ferromagnetic order at low temperature in Fig. 2b. Compared with high-temperature results, the bands above the Fermi level become sharp in the spin-up channel, while the bands remain blurred below the Fermi level. Conversely, in the spin-down channel, the upper Hubbard bands are retained, and the bands below the Fermi level become sharp. Additionally, the bands close to the Fermi level become more distinct in both spin channels, thus forming quasiparticles, which result in multiple peaks in DOS

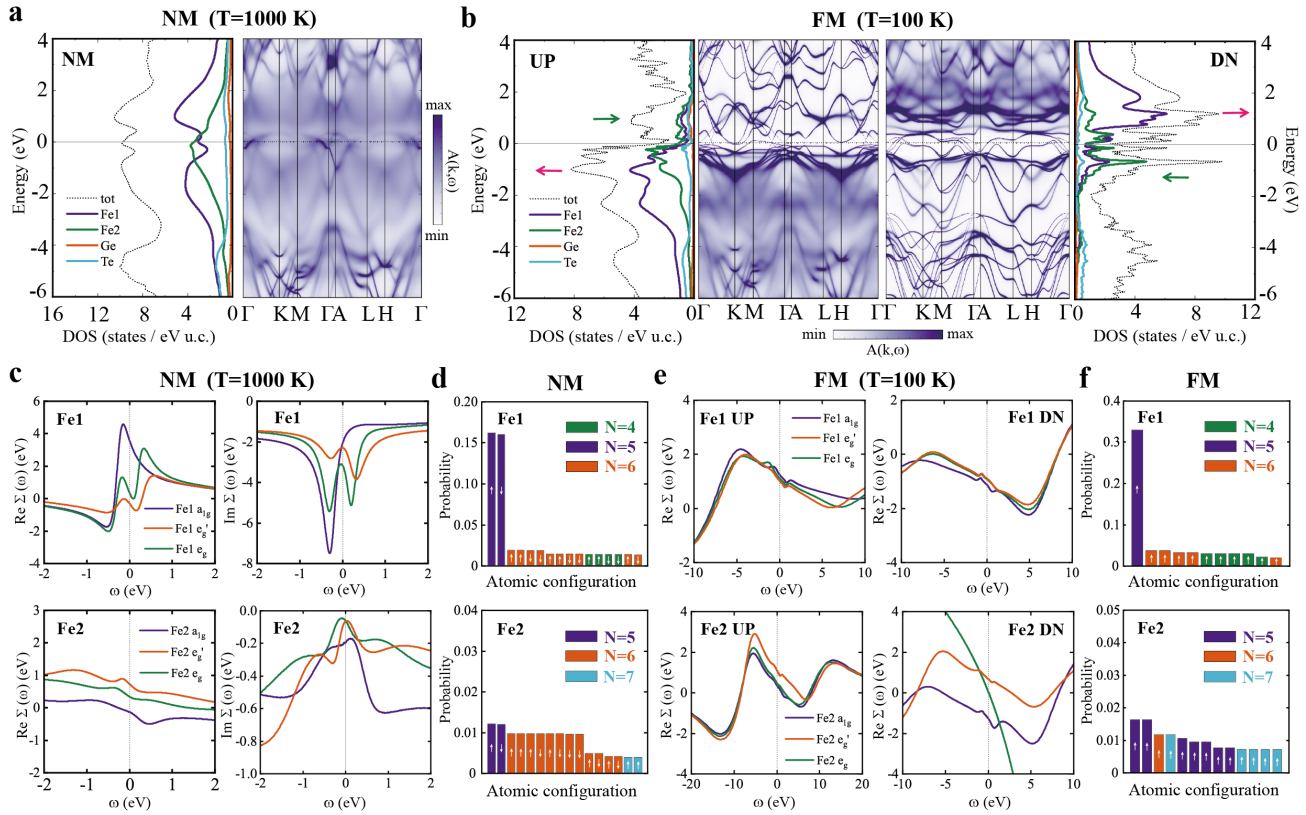


FIG. 2. The results of DFT+DMFT calculations of FGT at low and high temperatures. a,b, The calculated density of states and spectral functions in high-temperature non-magnetic order and low-temperature ferromagnetic order. In ferromagnetic order, the pink arrow in DOS shows the region of the spectral weight increasing, and the green arrow shows the spectral weight decreasing. c, The real and imaginary part of self-energy of Fe1 and Fe2 atoms in no-magnetic order. d, The several highest probabilities of the Fe atomic states from the impurity solver in non-magnetic calculations. The  $\uparrow$  arrow means  $S_z$  is positive and the  $\downarrow$  arrow means  $S_z$  is negative. e, The real part of self-energy of Fe1 and Fe2 atoms in ferromagnetic order. f, The several highest probabilities of the Fe atomic states from the impurity solver in ferromagnetic order.

around the Fermi level.

Here, we conclude several significant findings from further inspecting the microscopic processes in DFT+DMFT calculations. The most important observation is the spectral weight transfer in Hubbard bands, rather than the spin splitting suggested by the Stoner model. The colored arrows in Fig. 2b indicate the primary areas where spectral weight transfer occurs. This behavior is significantly different from those observed in DFT and DFT+U calculations. Previous ARPES experiments have strongly indicated this spectral weight transfer behavior [26]. They found that the spectral weight transfer is independent from the details of band structures, with the enhanced DOS at 500 meV and suppressed DOS at 200 meV below the Fermi energy in ferromagnetic state. Furthermore, recent ARPES measurements also show a weak temperature-dependent evolution of band shift, suggesting that local moments may play a crucial role in ferromagnetic order [27, 30]. In short, our proposed mechanism of spectral weight

transfer agrees well with ARPES measurements.

Secondly, a crossover is observed from high-temperature incoherence states to low-temperature coherence states in FGT, similar to what occurs in Hund metals [5, 10]. It is supported by recent optical experiments, indicating that Hund's coupling is essential in FGT [28]. The incoherent Hubbard bands originate from the significant spin scattering of Fe-*d* electrons, which can be clearly seen from the self-energy. The imaginary parts of the self-energy in Fig. 2c have significant values at zero frequency, approximately 2 eV for Fe1 and 0.1 eV for Fe2. However, at low temperatures, the imaginary parts of the self-energy approach zero, leading to the quasiparticle bands becoming distinct near the Fermi level, as shown in Fig. 2b. Furthermore, correlation effects result in the renormalization of the Fe-*d* bands near the Fermi level, which can be estimated from the real parts of self-energy with quasiparticle weight,  $Z = (1 - \partial_\omega \text{Re}\Sigma|_{\omega=0})^{-1}$ . Table I lists the mass enhancements ( $m^*/m_{\text{LDA}}$ ) of each orbital, calculated as  $Z^{-1}$  in DMFT. Our results demon-

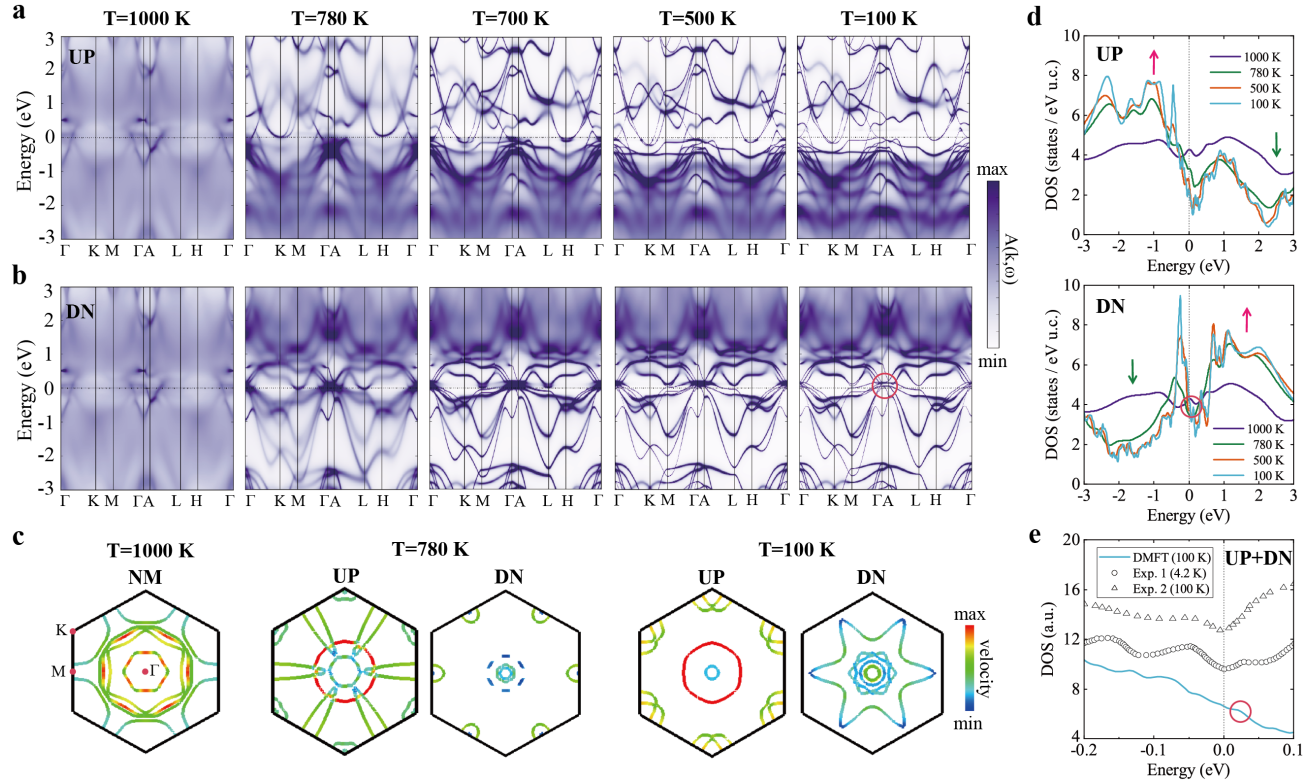


FIG. 3. The results of DFT+DMFT calculations of nonstoichiometric  $\text{Fe}_{2.82}\text{GeTe}_2$  with temperatures. a,b, The spectral functions of the spin-up and down channels with temperature from 1000 K to 100 K. c, The DFT+DMFT Fermi surfaces at different temperatures. d, The total density of states of spin-up and spin-down channels with varying temperatures. The colored arrows indicate the regions of spectral weight transfer. e, The calculated DOS is compared with STM measurements [22, 23].

strate that all the Fe-*d* orbitals are renormalized in both non-magnetic and ferromagnetic phases.

Thirdly, it is vital to shed light on the differences between FGT and other paramagnetic Hund metals [12, 40]. We focus on the detailed evolution of electronic structures during the magnetic transition. The highest atomic probabilities from the DMFT impurity solver is shown in Fig. 2d. Despite the fact that the average total spin of Fe1 and Fe2 are zero in paramagnetic order, the most significant cases are  $S_z = \pm 5/2$ , and they have the same probabilities. This implies that the Fe atoms have large local moments and fluctuate significantly over time. In the ferromagnetic state, the highest probabilities of Fe1 and Fe2 are primarily composed of only positive values of  $S_z$  in Fig. 2f, indicating the formation of magnetic order. Compared with paramagnetic Hund metals, we recognize that the long-range magnetic order will rapidly suppress the spin fluctuations, making it easier to form quasiparticles in the magnetic phase.

Finally, we recognize that Fe1 and Fe2 atoms exhibit different physical behavior, with Fe1 being described by Mottness and Fe2 characterized by Hundness. This difference is evident in the histogram associated with each

atomic configuration (Supplementary Information Fig.2). In Fig. 2d and f, Fe1 appear concentrated in a single charge state,  $N = 5$ , typical of the Mott type [10]. However, the histogram of Fe2 extend over many charge states, a direct signature of Hundness [5]. Another piece of evidence is the feature of DOS. The partial DOS of Fe1 has a pseudogap at the Fermi level between two broad humps near  $\pm 1$  eV in Fig. 2a, which is very similar to the Mott system  $\text{V}_2\text{O}_3$  [32]. Conversely, the partial DOS of Fe2 is characterized by a single broad feature, similar to the Hund metal  $\text{Sr}_2\text{RuO}_4$  [32]. We realize that the different physics of Fe1 and Fe2 may be due to their local environments, with the occupation of Fe1 and Fe2 being 5.0 and 5.8 in our DFT+DMFT calculations, corresponding to  $\text{Fe}^{3+}$  and  $\text{Fe}^{2+}$ . In multi-orbital correlated systems, Hund's coupling has a Janus-faced effect depending on the electron occupation [41]. As Fe1 are closed to half-filling, the Mott mechanism is promoted. In contrast, Fe2 are away from half-filling, so the Hund interaction is dominant. The valences of Fe atoms in our calculations are obtained using an exact double-counting scheme in DFT+DMFT calculations [42] and are consistent with previous predictions [17, 19].

TABLE I. The mass enhancements of Fe-orbitals at paramagnetic and ferromagnetic order in FGT.  $m_{\text{DFT}}$  represents the mass from DFT calculations. The respective Fe-3d states in FGT split into three classes: a  $d_{z^2}$ -like  $a_{1g}$  orbital, two degenerate  $e_g$  orbitals and two degenerate  $e_g$  orbitals. The  $\uparrow$  arrow means spin-up channel and the  $\downarrow$  arrow means spin-down channel.

		$m_{a_{1g}}^*/m_{\text{DFT}}$	$m_{e_g}^*/m_{\text{DFT}}$	$m_{e_g}^*/m_{\text{DFT}}$
PM	Fe1	9.1	4.5	7.6
	Fe2	1.5	1.8	2.3
FM	Fe1	$\uparrow$ 1.4	1.4	1.3
		$\downarrow$ 1.3	1.3	1.2
	Fe2	$\uparrow$ 1.4	1.4	1.3
		$\downarrow$ 1.6	1.4	2.0

### Effect of Fe vacancy on electronic structures

We have noticed a systematic discrepancy between our electronic structures of FGT and ARPES measurements [22, 27, 30]. Although surface effects could partially explain the discrepancy [43], the nonstoichiometry in FGT is significant due to the nonnegligible vacancy of Fe2 atoms [19, 21, 44]. Fig. 3 shows the temperature-dependent spectral functions in nonstoichiometric  $\text{Fe}_{3-\delta}\text{GeTe}_2$  ( $\delta \sim 0.18$ ). As expected, the main findings from stoichiometric FGT calculations are retained, including the spectral weight transfer in Hubbard bands, low-temperature quasiparticles with ferromagnetic order, and the coexistence of Hundness and Mottness. We observe that the band location remains relatively constant with temperature in Fig. 3a and b, which agrees well with recent APRES measurements [27, 30]. Furthermore, the Fermi surfaces in Fig. 3c consist of several circular and hexagonal-shaped Fermi pockets near the  $\Gamma$  point and elliptical-shaped pockets at the  $K$  point. Moreover, there is a complex-shaped Fermi pocket near the  $M$  point in the spin-down channel, which is consistent with experiments [22, 27, 30]. At low temperatures, some quasiparticle bands emerge in the spin-up channel near -0.5 eV, also observed in the ARPES experiments at the same binding energy [22, 27]. Fig. 3d shows that spectral weight transfer occurs as temperatures decrease. Meanwhile, the DOS has many small sharp peaks due to the complex flat quasiparticle bands formed at low temperatures. The agreement between our hole-doping calculations and ARPES measurements suggests the vital role of Fe2 vacancies in FGT.

### Origin of heavy fermion behavior in ferromagnets

Another critical issue is the emergence of heavy fermion behavior within ferromagnetic order [22], as the two often contradict each other. DFT+DMFT calculations in Fig. 3e show similar peaks near the Fermi level compared to STM measurements [22, 23]. As shown in Fig. 3d and

e, DFT+DMFT calculations illustrate some peaks just above the Fermi level, indicated by a red circle. As experiments suggest, these peaks possibly originate from the Kondo resonance [22, 23]. According to our calculations, these peaks come from the hole-like flat quasiparticle bands located at the  $\Gamma$  point, promoted by the rapid decrease of spin fluctuations in ferromagnetic order. Furthermore, as temperature decreases, the quasiparticle bands at the  $\Gamma$  point show strong hybridization with other relatively itinerant bands, where the partial DOS of Fe1, Fe2, and Ge atoms have similar shapes and peaks positions over a wide range (Supplementary Information Fig.3). These  $\Gamma$ -centered hole-like bands have a small Fermi velocity in Fig. 3c. Based on this evidence, we conclude that Hund's coupling can promote the formation of ferromagnetic order and heavy fermion behavior simultaneously. This mechanism demonstrates, for the first time, the complex competition and cooperation of magnetic order, Hundness, Mottness, and heavy fermion behavior in a detailed manner.

### Discussion

In strongly correlated physics, various exotic phenomena are closely related to the local moments of correlated atoms. One such outstanding material is the strongly correlated ferromagnetic metal FGT. However, the origin of magnetism in itinerant ferromagnets has been a controversial topic for several decades. As shown in Fig. 4, the Heisenberg model is used to describe the origin of magnetism in insulators [15]. In contrast, the Stoner model, based on the mean-field approximation,

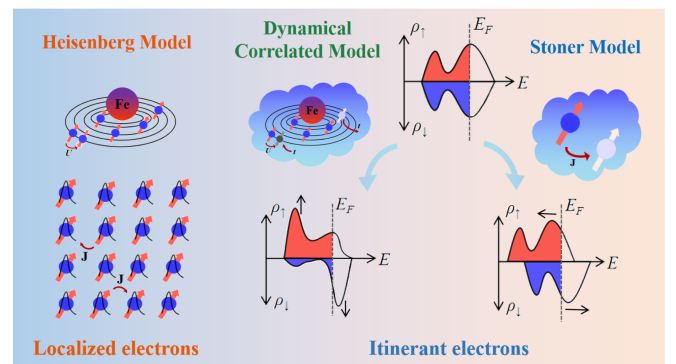


FIG. 4. The schematic diagram of electronic structure evolution in itinerant ferromagnets. The left and right sides show the local Heisenberg model and the itinerant Stoner model, respectively. In the Heisenberg model, the electrons are localized and cannot move through the crystal. In the Stoner model, electrons can move in the crystal, and the spin splitting comes from the different spin channels that move in the opposite direction. In correlated itinerant magnets, dynamical correlation effects will lead to collective excitation, making spectral weight transfer and quasiparticle forming through magnetic phase transition.

provides a phenomenological description of spin splitting in magnetic metals [16]. However, the Stoner model has been proven inadequate for these correlated systems [27, 30]. Even though Moriya and Kawabata attempted to consider spin fluctuations and correlation effects through self-consistent renormalization (SCR) theory, a detailed physical picture still needs to be provided [20, 45]. Our magnetic DFT+DMFT calculations aim to resolve this problem from the many-body dynamical correlation point of view. In ferromagnetic metals, Hund's coupling can produce collective excitation modes at low temperatures and create renormalized flat quasiparticle bands through dynamical correlation processes. Meanwhile, the spectral weight transfer occurs during magnetic phase transition. Additionally, the formation of ferromagnetic long-range order, in turn, promotes quasi-particle formation through positive feedback by rapidly reducing spin fluctuations in the microscopic mechanism. Ultimately, this leads to the simultaneous occurrence of spectral weight transfer, long-range magnetic order, and even other competing orders, such as heavy fermion behavior.

In summary, through systematic magnetic DFT+DMFT calculations on FGT, we have uncovered a new microscopic description of electronic structures in correlated ferromagnetic metals based on dynamical correlation effects. The Hund's coupling results in long-range ferromagnetic order accompanied by spectral weight transfer, rather than the spin splitting described by the Stoner model. This long-range magnetic order suppresses spin fluctuation rapidly, leading to the formation of renormalized quasiparticle bands. Our work also shows that heavy fermion behavior can be promoted by long-range magnetic order in itinerant magnets, through flat quasiparticle bands around the Fermi level further hybridizing with other itinerant bands at lower temperatures. In addition, the two Fe sites exhibit different physics, with Fe1 characterized by Mottness and Fe2 by Hundness, induced by the diversity of their atomic environment. Overall, our research indicates that multi-site itinerant magnets present a new frontier for discovering new quantum states and their competitions.

## Methods

### DFT calculations

The first-principles DFT calculations were performed using the projector-augmented wave (PAW) method [46], as implemented in the Vienna ab initio simulation package (VASP) [47] with the Perdew–Burke–Ernzerhof (PBE) functional [48]. The strongly correlated correction was considered with the GGA+U method, taking the suggested correlated values as  $U_{\text{eff}} = 4$  eV from previous work [24]. We also used doubly screened Coulomb correction (DSCC) approach to check the correlated values and got similar values [49]. The cut-off energy of the plane

wave basis-set was set to 500 eV. The Monkhorst-Pack grid was chosen as  $15 \times 15 \times 3$  to ensure convergence. The total energies were converged to  $10^{-8}$  eV. In our calculations, we adopted experimental lattice parameters with  $a = b = 3.99 \text{ \AA}$  and  $c = 16.33 \text{ \AA}$  [19].

### DFT+DMFT calculations

The DFT+DMFT calculations were employed to treat the electronic correlations of Fe-*d* orbitals. Full-potential linearized augmented plane-wave method implemented in the WIEN2k package was used in DFT+DMFT [50]. We employed the hybridization expansion continuous-time quantum Monte Carlo method as the impurity solver [51, 52] and applied the exact double-counting scheme [42]. The correlation parameters were set  $U = 5$  eV and  $J = 0.8$  eV, as suggested from earlier work [24]. We used the exact double-counting scheme, and it can get the proper occupied number of Fe atoms, consistent with experiments [17, 19]. To account for the effect of Fe vacancy, we modified our DFT+DMFT calculations by changing the number of electrons. Previous research has confirmed that changing electron numbers leads to similar results in constructing supercells with Fe2 vacancies [44, 53]. In order to perform magnetic DFT+DMFT calculations, we consider 10 Fe-*d* orbitals and break the symmetry with a change in the real-part energy of the initial self-energy of both two types of Fe atoms.

---

\* song\_haifeng@iapcm.ac.cn

† fuyang@ustb.edu.cn

- [1] Stewart, G. R. Heavy-fermion systems. *Rev. Mod. Phys.* **56**, 755-787 (1984).
- [2] Yang, Y.-F., Fisk, Z., Lee, H. O., Thompson, J. D. & Pines, D. Scaling the Kondo lattice. *Nature* **454**, 611-613 (2008).
- [3] Dagotto, E. Correlated electrons in high-temperature superconductors. *Rev. Mod. Phys.* **66**, 763-840 (1994).
- [4] Scalapino, D. J. A common thread: The pairing interaction for unconventional superconductors. *Rev. Mod. Phys.* **84**, 1383-1417 (2012).
- [5] Yin, Z. P., Haule, K. & Kotliar, G. Kinetic frustration and the nature of the magnetic and paramagnetic states in iron pnictides and iron chalcogenides. *Nat. Mater.* **10**, 932-935 (2011).
- [6] Haule, K. & Kotliar, G. Coherence–incoherence crossover in the normal state of iron oxypnictides and importance of Hund's rule coupling. *New J. Phys.* **11**, 025021 (2009).
- [7] Si, Q., Rabello, S., Ingersent, K. & Smith, J. L. Locally critical quantum phase transitions in strongly correlated metals. *Nature* **413**, 804-808 (2001).
- [8] Shen, B. et al. Strange-metal behaviour in a pure ferromagnetic Kondo lattice. *Nature* **579**, 51-55 (2020).
- [9] Shim, J. H., Haule, K. & Kotliar, G. Modeling the localized-to-itinerant electronic transition in the heavy fermion system CeIrIn<sub>5</sub>. *Science* **318**, 1615-1617 (2007).
- [10] Georges, A. & Kotliar, G. The Hund-metal path to strong electronic correlations. *Physics Today* **77**, 46-53 (2024).

[11] Georges, A., Medici, L. d. & Mravlje, J. Strong correlations from Hund's coupling. *Annu. Rev. Condens. Matter Phys.* **4**, 137-178 (2013).

[12] Haule, K., Shim, J. H. & Kotliar, G. Correlated electronic structure of  $\text{LaO}_{1-x}\text{F}_x\text{FeAs}$ . *Phys. Rev. Lett.* **100**, 226402 (2008).

[13] Yin, Z. P., Haule, K. & Kotliar, G. Magnetism and charge dynamics in iron pnictides. *Nat. Phys.* **7**, 294-297 (2011).

[14] Liu, M. et al. Nature of magnetic excitations in superconducting  $\text{BaFe}_{1.9}\text{Ni}_{0.1}\text{As}_2$ . *Nat. Phys.* **8**, 376-381 (2012).

[15] Heisenberg, W. Zur theorie des Ferromagnetismus. *Z. Phys.* **49**, 619 (1928).

[16] Stoner, E. C. Ferromagnetism. *Rep. Prog. Phys.* **11**, 43 (1947).

[17] Deng, Y. et al. Gate-tunable room-temperature ferromagnetism in two-dimensional  $\text{Fe}_3\text{GeTe}_2$ . *Nature* **563**, 94-99 (2018).

[18] Fei, Z. et al. Two-dimensional itinerant ferromagnetism in atomically thin  $\text{Fe}_3\text{GeTe}_2$ . *Nat. Mater.* **17**, 778-782 (2018).

[19] Deiseroth, H. J., Aleksandrov, Reiner, K., Kienle, C., L. & Kremer, R. K.  $\text{Fe}_3\text{GeTe}_2$  and  $\text{Ni}_3\text{GeTe}_2$  - Two new layered transition-metal compounds: crystal Structures, HRTEM investigations, and magnetic and electrical properties. *Eur. J. Inorg. Chem.* **2006**, 1561-1567 (2006).

[20] Chen, B. et al. Magnetic properties of layered itinerant electron ferromagnet  $\text{Fe}_3\text{GeTe}_2$ . *J. Phys. Soc. Jpn.* **82**, 124711 (2013).

[21] Verchenko, V. Y., Tsirlin, A. A., Sobolev, A. V., Presniakov, I. A. & Shevelkov, A. V. Ferromagnetic order, strong magnetocrystalline anisotropy, and magnetocaloric effect in the layered telluride  $\text{Fe}_{3-\delta}\text{GeTe}_2$ . *Inorg. Chem.* **54**, 8598-8607 (2015).

[22] Zhang, Y. et al. Emergence of Kondo lattice behavior in a van der Waals itinerant ferromagnet,  $\text{Fe}_3\text{GeTe}_2$ . *Sci. Adv.* **4**, eaao6791 (2018).

[23] Zhao, M. et al. Kondo holes in the two-dimensional itinerant Ising ferromagnet  $\text{Fe}_3\text{GeTe}_2$ . *Nano Lett.* **21**, 6117-6123 (2021).

[24] Zhu, J.-X. et al. Electronic correlation and magnetism in the ferromagnetic metal  $\text{Fe}_3\text{GeTe}_2$ . *Phys. Rev. B* **93**, 144404 (2016).

[25] Kim, K. et al. Large anomalous Hall current induced by topological nodal lines in a ferromagnetic van der Waals semimetal. *Nat. Mater.* **17**, 794-799 (2018).

[26] Zhuang, H. L., Kent, P. R. C. & Hennig, R. G. Strong anisotropy and magnetostriction in the two-dimensional Stoner ferromagnet  $\text{Fe}_3\text{GeTe}_2$ . *Phys. Rev. B* **93**, 134407 (2016).

[27] Xu, X. et al. Signature for non-Stoner ferromagnetism in the van der Waals ferromagnet  $\text{Fe}_3\text{GeTe}_2$ . *Phys. Rev. B* **101**, 201104(R) (2020).

[28] Corasaniti, M. et al. Electronic correlations in the van der Waals ferromagnet  $\text{Fe}_3\text{GeTe}_2$  revealed by its charge dynamics. *Phys. Rev. B* **102**, 161109(R) (2020).

[29] Bao, S. et al. Neutron spectroscopy evidence on the dual nature of magnetic excitations in a van der Waals metallic ferromagnet  $\text{Fe}_{2.72}\text{GeTe}_2$ . *Phys. Rev. X* **12**, 011022 (2022).

[30] Wu, H. et al. Spectral evidence for local-moment ferromagnetism in the van der Waals metals  $\text{Fe}_3\text{GaTe}_2$  and  $\text{Fe}_3\text{GeTe}_2$ . *Phys. Rev. B* **109**, 104410 (2024).

[31] Song, Y. et al. A Mott insulator continuously connected to iron pnictide superconductors. *Nat. Commun.* **7**, 13879 (2016).

[32] Deng, X. et al. Signatures of Mottness and Hundness in archetypal correlated metals. *Nat. Commun.* **10**, 2721 (2019).

[33] Kim, T. J., Ryee, S. & Han, M. J.  $\text{Fe}_3\text{GeTe}_2$ : a site-differentiated Hund metal. *npj Comput. Mater.* **8**, 245 (2022).

[34] Bai, X. et al. Antiferromagnetic fluctuations and orbital-selective Mott transition in the van der Waals ferromagnet  $\text{Fe}_{3-x}\text{GeTe}_2$ . *Phys. Rev. B* **106**, L180409 (2022).

[35] Kondo, S. et al.  $\text{LiV}_2\text{O}_4$ : a heavy fermion transition metal oxide. *Phys. Rev. Lett.* **78**, 3729-3732 (1997).

[36] Cheng, J.-G. et al. Possible Kondo physics near a metal-insulator crossover in the a-site ordered perovskite  $\text{CaCu}_3\text{Ir}_4\text{O}_{12}$ . *Phys. Rev. Lett.* **111**, 176403 (2013).

[37] Takegami, D. et al.  $\text{CaCu}_3\text{Ru}_4\text{O}_{12}$ : A high-Kondo-temperature transition-metal oxide. *Phys. Rev. X* **12**, 011017 (2022).

[38] Kotliar, G. et al. Electronic structure calculations with dynamical mean-field theory. *Rev. Mod. Phys.* **78**, 865-951 (2006).

[39] Haule, K., Yee, C. & Kim, K. Dynamical mean-field theory within the full-potential methods: Electronic structure of  $\text{CeIrIn}_5$ ,  $\text{CeCoIn}_5$ , and  $\text{CeRhIn}_5$ . *Phys. Rev. B* **81**, 195107 (2010).

[40] Mravlje, J. et al. Coherence-incoherence crossover and the mass-renormalization puzzles in  $\text{Sr}_2\text{RuO}_4$ . *Phys. Rev. Lett.* **106**, 096401 (2011).

[41] Medici, L. de', Mravlje, J. & Georges, A. Janus-faced influence of Hund's rule coupling in strongly correlated materials. *Phys. Rev. Lett.* **107**, 256401 (2011).

[42] Haule, K. Exact double counting in combining the dynamical mean field theory and the density functional theory. *Phys. Rev. B* **115**, 196403 (2007).

[43] Wang, Y.-C. et al. First-principles study of the role of surface in the heavy-fermion compound  $\text{CeRh}_2\text{Si}_2$ . *Phys. Rev. B* **103**, 165140 (2021).

[44] Jang, S. W. et al. Origin of ferromagnetism and the effect of doping on  $\text{Fe}_3\text{GeTe}_2$ . *Nanoscale* **12**, 13501 (2020).

[45] Hatatani, M. & Moriya, T. Ferrromagnetic spin fluctuations in two-dimensional metals. *J. Phys. Soc. Jpn.* **64**, 3434 (1995).

[46] Blöchl, P. E. Projector augmented-wave method. *Phys. Rev. B* **50**, 17953-17979 (1994).

[47] Kresse, G. & Furthmüller, J. Efficient iterative schemes for ab initio total-energy calculations using a plane-wave basis set. *Phys. Rev. B* **54**, 11169-11186 (1996).

[48] Perdew, J. P., Burke, K. & Ernzerhof, M. Generalized gradient approximation made simple. *Phys. Rev. Lett.* **77**, 3865-3868 (1996).

[49] Liu, B., Wang, Y., Liu, Y., Liu, H. & Song, H. Doubly screened Coulomb correction approach for strongly correlated systems. *J. Phys. Chem. Lett.* **14**, 8930-8939 (2023).

[50] Blaha, P. et al. *WIEN2K, An augmented plane wave + local orbitals program for calculating crystal properties* (Karlheinz Schwarz, Techn. Universität Wien, Austria, 2023).

[51] Werner, Comanac, P. A., Medici, L. de', Troyer, M. & Millis, A. J. Continuous-time solver for quantum impurity models. *Phys. Rev. Lett.* **97**, 076405 (2006).

[52] Haule, K. Quantum Monte Carlo impurity solver for cluster dynamical mean-field theory and electronic structure

calculations with adjustable cluster base. *Phys. Rev. B* **75**, 155113 (2007).

[53] Lee, J.-E. et al. Electronic structure of above-room-temperature van der Waals ferromagnet  $\text{Fe}_3\text{GaTe}_2$ . *Nano Lett.* **23**, 11526-11532 (2023).

### Acknowledgements

The authors thank Yingying Cao, Beilei Liu, Huican Mao and Kun Zhai for the fruitful discussions. This work is supported by the National Natural Science Foundation of China (Grant Nos. U2230401, 12204033, 52371174), the National Key Research and Development Program of China (Grant No. 2021YFB3501503), the Founda-

tion of LCP, the Fundamental Research Funds for the Central Universities (Grant No. FRF-TP-22-097A1) and the Young Elite Scientist Sponsorship Program by BAST (Grant No. BYESS2023301). We thank the Tianhe platforms at the National Supercomputer Center in Tianjin.

### Author contributions

F. T. and H. S. conceived the idea and supervised the project; Y. X. and Y. W. performed the calculations; X. J., Y. L. and H. L. participated in the discussions. Y. X. wrote the paper with input from all authors. All authors contributed to the interpretation of the data and revised the paper. Y. X. and Y. W. contributed equally to this work.